DOI: 10.1002/ejic.200500830

Reaction of the Heteronuclear Cluster $[Cp^*IrRu_3(\mu\text{-}H)_2(CO)_{10}]$ with Alkynes: Stereoselective Binding

Padmamalini Srinivasan[a] and Weng Kee Leong*[a]

Keywords: Heterometallic complexes / Ruthenium / Iridium / Alkynes / Stereoselectivity

The reaction of the heteronuclear cluster $[Cp^*IrRu_3(\mu\text{-}H)_2(CO)_{10}]$ (**1**) with the symmetrical alkynes RCCR (R = Ph, Et) afforded the butterfly clusters $[Cp^*IrRu_3(CO)_9(RCCR)]$ (**2**) and the trinuclear clusters $[Cp^*IrRu_2(CO)_7(RCCR)]$ (**3**) and $[Ru_3(CO)_8(C_4R_4)]$ (**4**). The clusters **2** and **3** have the alkyne aligned parallel to an Ru–Ir bond. The reaction of **1** with unsymmetrical alkynes also afforded stereoselective binding of the alkyne such that the bulkier substituent was pointing away from the Cp^*Ir moiety; with PhCCH, however, all three stereoisomers were obtained. With the bis-silylated alkynes (R = $SiMe_3$, $SiEt_3$), loss of one trialkylsilyl group occurred to give $[Cp^*IrRu_3(CO)_9(HCCR)]$ and $[Ru_3(CO)_9(\mu\text{-}H)(CCR)]$ (**5**).

Introduction

Mixed-metal alkyne clusters have been of interest because of their catalytic potential in hydrogenation reactions,[1] as models for the carbon–carbon triple bond activation on metal surfaces and for chemisorption of small molecules on metal surfaces,[2] as well as precursors to bimetallic particles.[3] The reaction of tetrahedral clusters with alkynes often results in cluster opening to give "butterfly" structures,[4] where the M_3M' skeleton takes the form of a butterfly and the alkyne C_2 unit binds to the metal framework in a μ_4-η^2 fashion to form a quasi-octahedral $M_3M'C_2$ skeleton.[5] The total electron count for these clusters are best considered using the Wade's system, i.e., as octahedral $M_3M'C_2$ clusters, with each CR unit donating three electrons to the skeletal bonding. They are therefore 62-electron "electron precise" butterfly or 14-electron *closo* octahedral clusters;[6] use of the EAN rule predicts unsaturation, which is not in agreement with their reactivity and hence discouraged.[7]

Three isomers are possible for the $M_3M'C_2$ skeleton and for the coordinated alkynes (Figure 1). The alkyne can be disposed parallel to a heterometallic MM′ bond (a) or to a homometallic MM bond (b); these are related as hinge-apex isomers. The orientation of the alkyne with respect to the hinge bond can also be different, such as in (a) and (c), which are related as (*cis*,*trans*) alkyne isomers.

Most reactions of heterometallic tetrahedral clusters with alkynes afforded butterfly clusters exhibiting either hinge-apex or alkyne, or both types of isomerism. In some cases, however, the reactions were found to be highly stereoselective. For example, the reaction of $[CpMRu_3(CO)_{12}]^-$ (M = W, Mo), $[IrRu_3(\mu\text{-}H)(CO)_{13}]$ and $[IrRu_3(CO)_{13}]^-$ towards internal alkynes afforded ‖M–Ru (M = W, Mo and Ir) clusters with alkyne insertion into the Ru–Ru bond as the only product.[8] However, the reaction of $[CpMRu_3(CO)_{12}]^-$ (M = W, Mo) clusters with phenyl acetylene afforded ‖M–Ru *cis* and *trans* isomers,[8a] while the reaction of $[FeRu_3(\mu\text{-}H)_2(CO)_{13}]$ with alkynes afforded hinge-apex as well as alkyne isomers; isomerisation of the ‖Fe–Ru to the ‖Ru–Ru isomer occurred on heating.[9] In the reaction of $[Cp^*RhRu_3(\mu\text{-}H)_4(CO)_9]$ with alkynes, the isomer with the heterometal atom at the wingtip (‖Ru–Ru) was obtained as the only isomer, while the Cp analogue afforded both hinge-apex isomers (‖Rh–Ru and ‖Ru–Ru). However, it was observed that the ‖Rh–Ru isomer converted into the ‖Ru–Ru isomer during purification of the product on TLC plates.[10] In both the FeRu and RhRu systems, the reverse isomerisation was not facile. This suggested that for these two systems, the isomer with the heterometal atom in the hinge was the kinetically favored product and that with the heterometal atom in the wingtip was the thermodynamically more stable product.

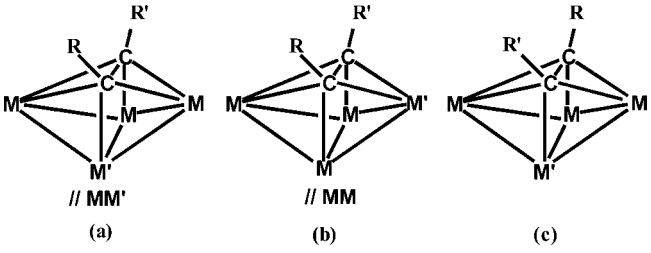

Figure 1. Isomers in $M_3M'C_2$ clusters.

Heterometallic clusters like the previously reported $[CpRhRu_3(\mu\text{-}H)_4(CO)_9]$ are attractive as they allow for the study of site selectivity in the binding of alkynes, particularly unsymmetrical alkynes; the Cp serves as a ligand which allows for stereoelectronic influence on the cluster.

[a] Department of Chemistry, National University of Singapore, Kent Ridge, Singapore 119260

However, this cluster was known to fragment readily under the reaction conditions,[10] and we thus sought to examine the reactivities of some heavier relatives, viz., $[Cp^*IrM_3(\mu\text{-}H)_2(CO)_{10}]$ [M = Ru (**1**) or Os], which we have recently synthesised,[24] in the hope that the third-row elements would lend stability to the cluster core. Our investigations with the cluster **1** are reported here.

Results and Discussion

Reactions of 1 with Alkynes: The thermal reaction of **1**, with the symmetrical alkynes RCCR (R = Ph, Et) in hexane afforded a dark red solution from which three compounds, viz., $[Cp^*IrRu_3(CO)_9(RCCR)]$ (**2**), $[Cp^*IrRu_2(CO)_7(RCCR)]$ (**3**), and $[Ru_3(CO)_8(C_4R_4)]$ (**4**) were isolated (Scheme 1).

All the products have been completely characterised, including by single-crystal X-ray crystallographic studies. The clusters **4a** and **4b** have been reported previously,[11] including the X-ray crystal structure in the case of the former.[12] The ORTEP plots for **2a**, **3a** and **4b** are shown in Figure 2, Figure 3 and Figure 4, respectively. The alkyne butterfly clusters **2** have the alkyne C≡C bond parallel to an Ru–Ir hinge; their structural discussion will follow later.

The gross structural features of **4b** are very similar to those of **4a**.[11a] As has been observed there, the Ru_3C_4 unit is in an approximately pentagonal bipyramidal arrangement, the Ru–Ru bonds are rather short and attributable to the two bridging carbonyl groups, and the double bonds of the butadiene-1,4-diyl moiety are delocalised over the three C–C bonds although the central bond is marginally longer. However, the asymmetry observed in **4b** is statistically more significant than those observed in **4a** because of the lower e.s.d.s. Thus the two Ru–Ru bonds are different and the difference in bond lengths between the central C–C bond of the butadiene-1,4-diyl moiety compared to the other two is now statistically significant.

A common atomic numbering scheme and selected bond parameters for **3a** and **3b** are given in Table 1. Both the clusters **3** are Ru_2Ir clusters with an electron count of 48; their structural features are similar. There is an asymmetrical carbonyl bridge, and the alkyne ligand is coordinated in a μ_3-η^2 fashion over the Ru_2Ir triangle, with the alkyne C–C bond parallel to the Ru–Ir bond bridged by the carbonyl. This type of bonding mode of an alkyne has been observed in a number of clusters.[13] The longest metal–metal bond

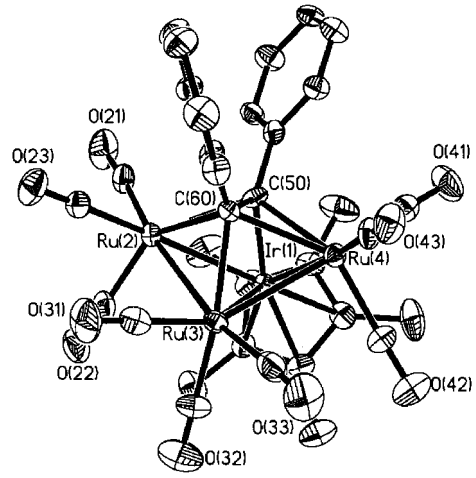

Figure 2. ORTEP diagram of **2a**. Thermal ellipsoids are drawn at the 50% probability level. The phenyl hydrogen atoms are omitted for clarity.

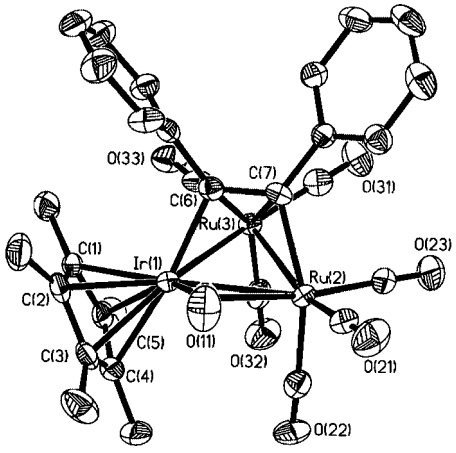

Figure 3. ORTEP diagram of **3a**. Thermal ellipsoids are drawn at 50% probability level. The phenyl hydrogen atoms are omitted for clarity.

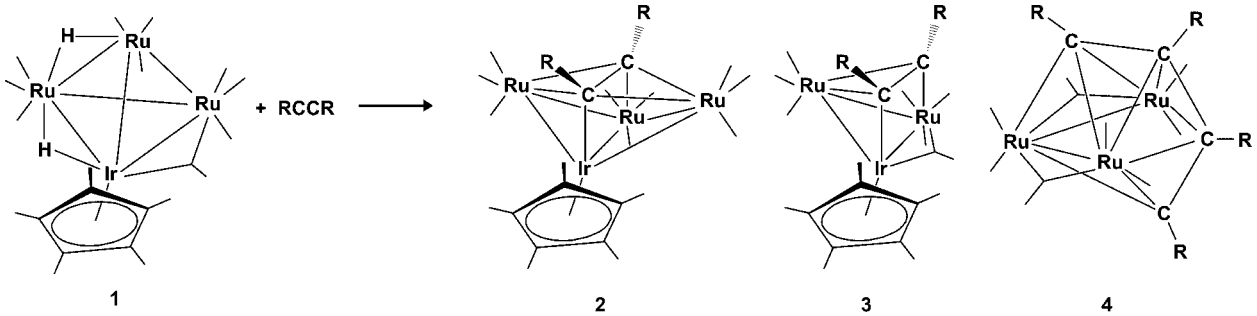

	2	3	4
a R = Ph	24%	17%	37%
b R = Et	41%	13%	33%

Scheme 1.

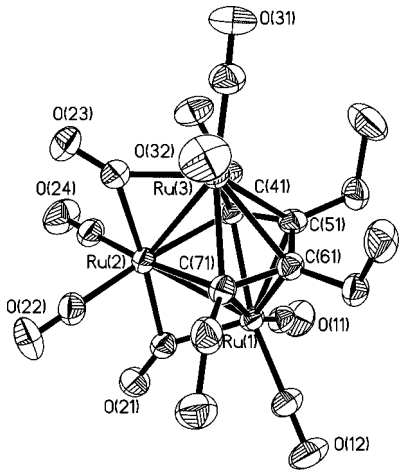

Figure 4. ORTEP diagram and selected bond parameters of **4b**. Thermal ellipsoids are drawn at 50% probability level. Organic hydrogen atoms are omitted for clarity. Ru(1)–Ru(2) = 2.6646(4) Å; Ru(2)–Ru(3) = 2.6741(4) Å; Ru(1)–C(41) = 2.275(3) Å; Ru(1)–C(51) = 2.297(3) Å; Ru(1)–C(61) = 2.300(3) Å; Ru(1)–C(71) = 2.317(3) Å; Ru(2)–C(41) = 2.192(3) Å; Ru(2)–C(71) = 2.188(3) Å; Ru(3)–C(41) = 2.315(3) Å; Ru(3)–C(51) = 2.363(3) Å; Ru(3)–C(61) = 2.352(3) Å; Ru(3)–C(71) = 2.252(3) Å; C(41)–C(51) = 1.440(5) Å; C(51)–C(61) = 1.479(5) Å; C(61)–C(71) = 1.444(5) Å; Ru(1)–Ru(2)–Ru(3) = 88.967(11)°.

is Ir(1)–Ru(2), which is bridged by the carbonyl and is also parallel to the alkyne C–C bond; this bond is significantly longer than the other two. The alkyne C–C bond lengths at ca. 1.40 Å have clearly lost their triple bond character; the bond order is less than two.[14]

Table 1. Common atomic numbering scheme and selected bond parameters for **3a** and **3b**.

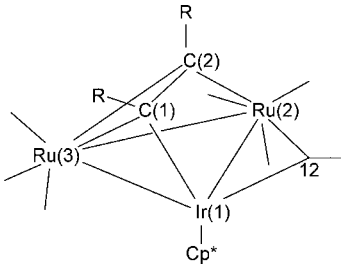

	3a (R = Ph)	**3b** (R = Et)
Bond lengths [Å]		
Ir(1)–Ru(2)	2.7977(5)	2.8034(5)
Ir(1)–Ru(3)	2.7091(5)	2.7022(5)
Ru(2)–Ru(3)	2.6852(6)	2.6892(7)
Ir(1)–C(1)	2.090(6)	2.067(6)
Ru(2)–C(2)	2.116(5)	2.094(7)
Ru(3)–C(1)	2.196(5)	2.196(6)
Ru(3)–C(2)	2.250(5)	2.214(6)
Ir(1)–C(12)	1.880(6)	1.893(7)
Ru(2)–C(12)	2.422(6)	2.362(7)
C(1)–C(2)	1.393(8)	1.402(9)
C(12)–O(12)	1.160(7)	1.164(8)
Bond angles [°]		
Ru(2)Ir(1)Ru(3)	58.342(14)	58.443(16)
Ir(1)Ru(2)Ru(3)	59.178(14)	58.896(15)
Ir(1)Ru(3)Ru(2)	62.481(15)	62.660(16)
Ir(1)C(12)O(12)	153.0(5)	150.6(6)
Ru(2)C(12)O(12)	126.9(5)	127.8(5)

The yields of the clusters **3** increased at the expense of that for clusters **2** when the reaction time was prolonged. This suggested that **3** were derived from the butterfly alkyne clusters **2**. This was also supported by the observation that thermolyses of **2a** and **2b** afforded **3a** and **3b**, respectively. Furthermore, we have also found that the UV photolyses of solutions of **2** yielded **3**. Thus the butterfly alkyne clusters were not very stable at high temperatures or under photolytic conditions, and were prone to undergo fragmentation to yield the stable triangular clusters. However, neither thermolysis nor photolysis yielded the triruthenium clusters **4**, which indicated that **2** were not the precursors. Similarly, we have found that $[Cp^*Ir(CO)_2]$ did not react with **4a** or **4b** under thermolytic or photolytic conditions. Thus the formation of clusters **4** involved a different pathway from that leading to **2** and **3**.

The reaction of **1** with the unsymmetrical alkynes *t*BuCCMe, 1-hexyne and Me_3SiCCH, however, gave only very low yields of the alkyne butterfly clusters **2** (Scheme 2). The reaction with 1-hexyne was particularly poor, and the amount of material obtained was very little, although the IR spectral profile suggested that it had a similar structure to **2c**.[15] For Me_3SiCCH, the known triruthenium cluster $[Ru_3(CO)_9(\mu\text{-}H)(C_2SiMe_3)]$ (**5a**) was also obtained.[16] With the exception of **2d**, the molecular structures of all the products have been determined by single-crystal X-ray crystallographic studies, albeit that for **5a** has already been reported.[17,18] The ORTEP plot for **2c** is shown in Figure 5, and it shows that the C≡C bond of the alkyne is again parallel to an Ru–Ir hinge, and the less bulky group of the alkyne is *cis* to the Cp*Ir. The ^{1}H NMR spectrum of **2c** did not show the presence of isomers. Hence the binding of the unsymmetrical alkyne appeared to be highly stereoselective. Monitoring of the reaction using infrared spectroscopy showed that strong peaks attributable to $[Cp^*Ir(CO)_2]$ were formed, suggesting fragmentation of the cluster.

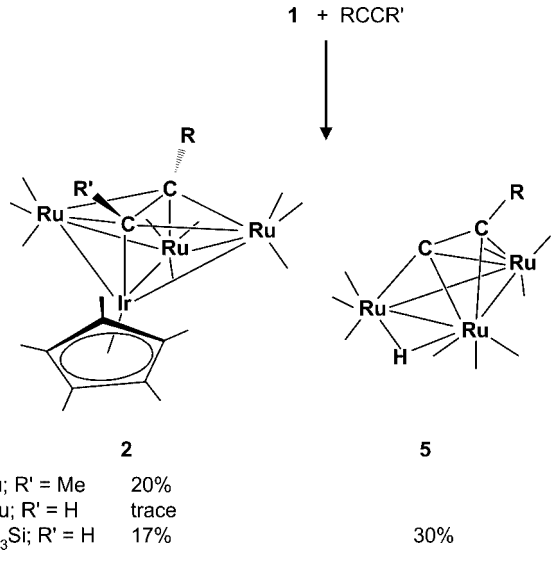

Scheme 2.

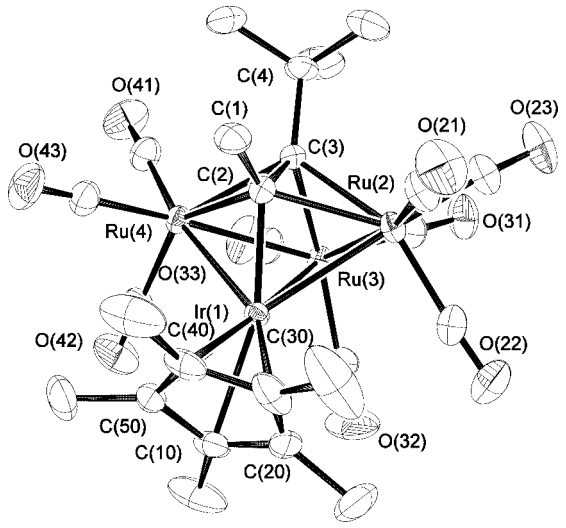

Figure 5. ORTEP diagram of **2c**. Thermal ellipsoids are drawn at 50% probability level. Organic hydrogen atoms are omitted for clarity.

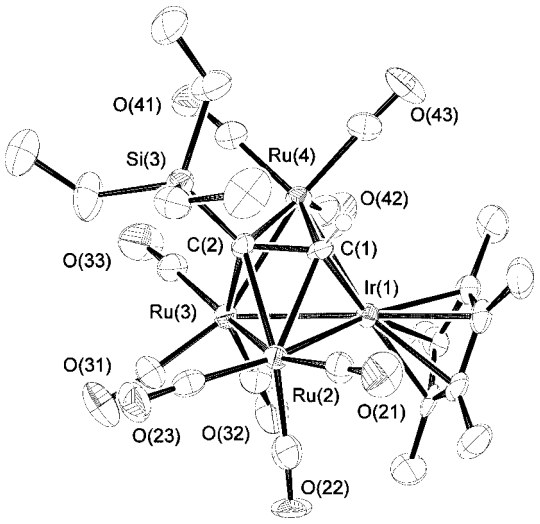

Figure 6. ORTEP diagram of **2f**. Thermal ellipsoids are drawn at 50% probability level. Organic hydrogen aotms are omitted for clarity.

Somewhat surprisingly, the thermal reaction of **1** with the bis-silylated alkynes $R_3SiCCSiR_3$ (R = Me, Et) in hexane afforded two products which were analogous (or identical for R = Me) to those for Me_3SiCCH (Scheme 3). The identity of the clusters **2e** and **2f** have been confirmed by complete characterisation, including by single-crystal X-ray crystallographic studies; the ORTEP plot for **2f** is shown in Figure 6.

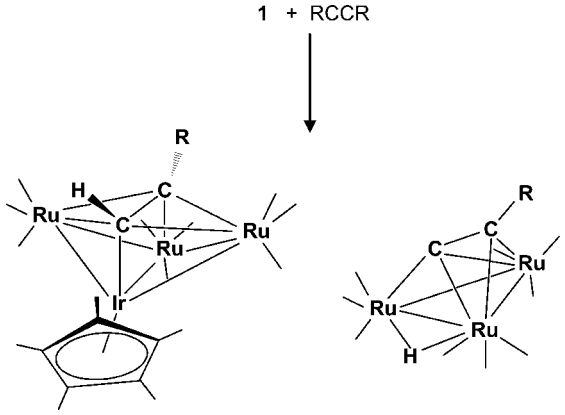

Scheme 3.

The replacement of one trialkylsilyl group by hydrogen was also clearly supported by the ^{1}H NMR and FAB MS data; the singlets at $\delta \approx 10.5$ ppm corresponded to the alkenic hydrogen atoms on the alkynes and were in agreement with similar compounds reported in the literature.[18] Monitoring of the reaction with $Me_3SiCCSiMe_3$ by ^{1}H NMR spectroscopy showed that the trimethylsilyl group was lost during the reaction and not during workup. GC analysis of an aliquot of the crude reaction mixture suggested that the trimethylsilyl group was lost as octamethyltrisiloxane, which suggested that the hydrogen may have originated from trace amounts of water. However, the desilylation product was observed in almost similar yields even when the reaction was carried out with thoroughly dried solvents and glassware. Since [Cp*Ir(CO)$_2$] is known to bring about C–H activation of hydrocarbons, it is also possible that the Cp*Ir(CO) fragment in these clusters may be responsible for the hydride exchange with $SiMe_3$ group.

Desilylation has been reported by Schneider and co-workers in their attempt to synthesize Fe–Ni heteronuclear clusters by the vaporisation of nickel atoms into a solution of (bistrimethylsilyl)acetylene and [Fe(CO)$_5$]; the reaction had unexpectedly afforded the cluster [Fe$_3$(CO)$_9$(μ-H)(C≡CSiMe$_3$)], and it was suggested that cleavage might have occurred during chromatographic work-up.[19] Vahrenkamp and co-workers have also reported desilylation in the reaction of [RuCo$_2$(CO)$_{11}$] with $Me_3SiC{\equiv}CMe$. The initial product, [RuCo$_2$(CO)$_9$(μ$_3$-$Me_3SiC{\equiv}CMe$)], formed in the reaction underwent subsequent desilylation to give [RuCo$_2$(CO)$_9$(μ$_3$-HC≡CMe)].[20]

In contrast to the highly stereoselective reactions with the other unsymmetrical alkynes above, the reaction of **1** with phenylacetylene afforded three isomeric alkyne butterfly clusters as red crystalline products (Scheme 4). The major product, obtained in 28% yield, was identified as [Cp*IrRu$_3$(CO)$_9$(PhCCH)] (**2g$_3$**); it has been characterised spectroscopically and analytically, as well as by a single-crystal X-ray structure analysis. The ORTEP plot of **2g$_3$** is shown in Figure 7, and it shows that the alkyne C≡C bond is parallel to an Ru–Ru hinge. The other two products were obtained in very low yields. A single-crystal X-ray structural study on **2g$_2$** showed it to be a hinge-apex isomer of **2g$_3$** in which the bulkier Ph group of the alkyne is oriented *cis* to the Cp*Ir; the ORTEP plot for **2g$_2$** is shown in Figure 8. The IR spectrum of the third product, **2g$_1$**, shows a

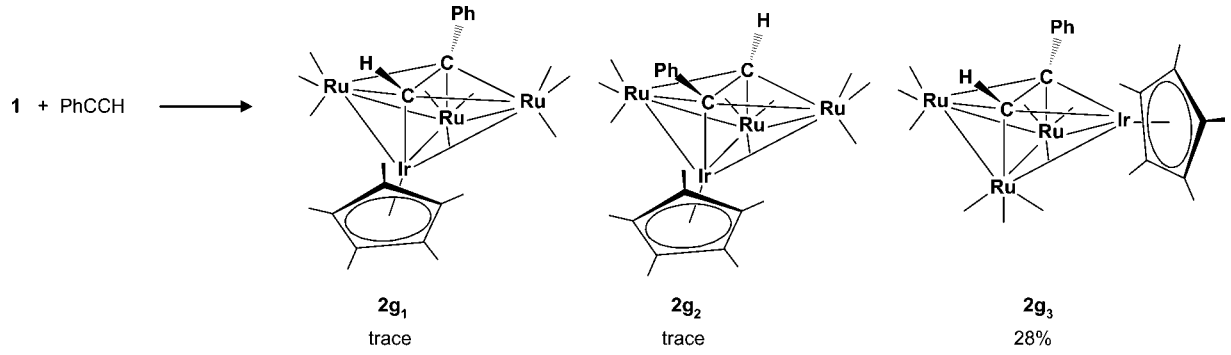

Scheme 4.

pattern similar to that of **2a**–**f**. The ^{1}H NMR characteristics are consistent with the assumption of a cluster-bound PhCCH. The multiplet between δ = 7.00 and 7.77 ppm is due to aromatic protons, the singlet at δ = 1.82 ppm can be assigned to Cp* methyl protons, and the singlet at δ = 10.58 ppm corresponds to the alkyne C–H. The MS is also consistent with structures like those observed for $\mathbf{2g_2}$ and $\mathbf{2g_3}$. Based on these spectroscopic characteristics it was thus tentatively identified as a third isomer in which the alkyne C≡C bond is parallel to an Ru–Ir hinge, and the bulkier Ph group of the alkyne is *trans* to the Cp*Ir, i.e., similar to **2c**–**f**.

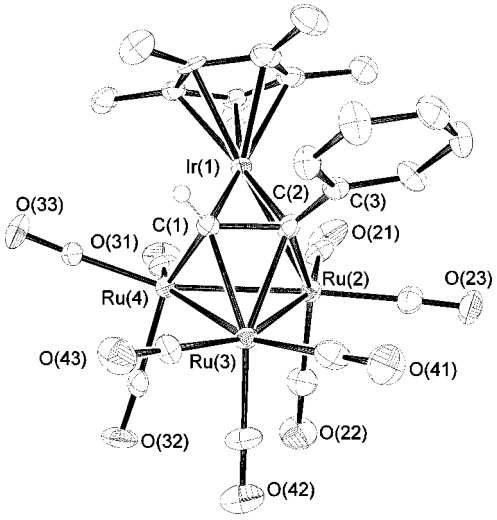

Figure 7. ORTEP diagram of $\mathbf{2g_3}$. Thermal ellipsoids are drawn at 50% probability level. Organic hydrogen atoms are omitted for clarity.

In the reaction of **1** with internal alkynes, only the ‖Ru–Ir isomers were observed; prolonged heating of this isomer did not lead to isomerisation but to cluster fragmentation instead. In contrast, the reaction with phenylacetylene yielded the ‖Ru–Ru isomer $\mathbf{2g_3}$ as the major product; the ‖Ru–Ir *cis* and ‖Ru–Ir *trans* isomers were obtained as minor products. It was observed by IR spectroscopy that a solution of $\mathbf{2g_3}$ converted slowly to $\mathbf{2g_1}$ and $2g_2$ on standing. Likewise, monitoring of a deuterated benzene solution of

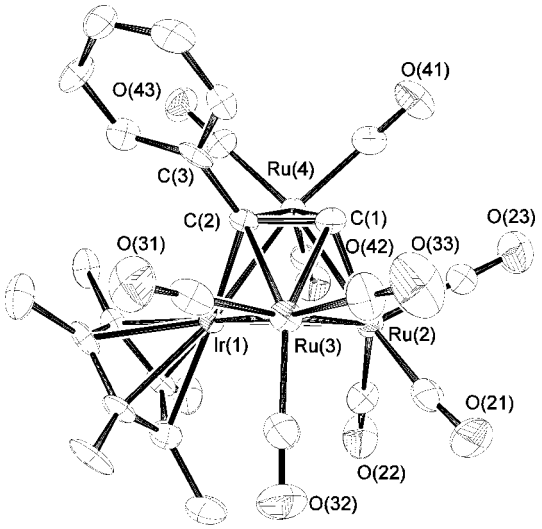

Figure 8. ORTEP diagram of $\mathbf{2g_2}$. Thermal ellipsoids are drawn at 50% probability level. Organic hydrogen atoms are omitted for clarity.

$\mathbf{2g_3}$ by ^{1}H NMR at ambient temperature indicated the slow formation of two new singlets at δ = 1.82 and 1.87 ppm, assignable to the Cp* signals of $\mathbf{2g_1}$ and $\mathbf{2g_2}$, respectively, as well as singlets at δ = 10.58 and 11.37 ppm, due to the respective C–H protons of the phenylacetylene. However, complete conversion to either $\mathbf{2g_1}$ or $\mathbf{2g_2}$ was not observed even after a month. Prolonged heating of $\mathbf{2g_3}$ finally afforded a 1.2:1.0:5.4 equilibrium mixture of $\mathbf{2g_1}$/$\mathbf{2g_2}$/$\mathbf{2g_3}$. This indicated clearly that the equilibrium lies towards the ‖Ru–Ru isomer $\mathbf{2g_3}$, i.e., that it was the thermodynamically most stable isomer. This is in agreement with the earlier observations on the $[FeRu_3(\mu\text{-}H)_2(CO)_{13}]$ and $[Cp/Cp^*RhRu_3(\mu\text{-}H)_4(CO)_9]$ systems.[9,10]

As a natural extension from the above reactions with alkynes, we attempted the reaction of **1** with 1-hexene to see if cluster-olefin complexes may be prepared, but none could be isolated. Instead, we found that the cluster-catalysed isomerisation of 1-hexene gave a mixture of 2- and 3-hexenes. However, we have monitored the reaction by ^{1}H NMR spectroscopy and found that complete isomerisation was not achieved even after many hours.

Structural Discussions on 2

The clusters **2** have been studied crystallographically; selected bond parameters using a common atomic numbering scheme were presented in Table 2. With the exception of **2g$_3$**, the alkyne is disposed parallel to the hinge heterometallic bond, with the torsion angle between the carbon–carbon backbone and the Ir(1)–Ru(3) edge close to 0° [torsion angles ranging between –0.7 to 1.9°]. This hinge Ir–Ru bond is also the longest of the metal–metal bonds, as has been generally found in M_4C_2 butterfly clusters.[21] The Ir–Ru bond lengths in general are, however, comparable to Ir–Ru bond lengths reported in the literature [Ir–Ru = 2.4972–2.9882 Å].[22] Also evident is the loss of multiple-bond character in the alkyne C–C bond; this length is surprisingly consistent across the different clusters, averaging 1.45 Å and with the range of values well within the experimental errors, despite the variation in substituents. However, there is a clear trend that the alkyne is closer to the iridium than to the ruthenium, as has been observed for clusters **3** above; this is consistent with the difference in the metal–metal bond lengths of [Ir$_4$(CO)$_{12}$] and [Ru$_3$(CO)$_{12}$] (mean of 2.693 and 2.853 Å, respectively).[23] The effect of asymmetry in the alkyne is also evident in the $M_{wingtip}$–C_{alkyne} bond lengths; the M–C distance to the C_{alkyne} carrying the bulkier substituent is longer than that to the C_{alkyne} carrying the less bulky group. This difference ranges from 0.04 to 0.08 Å, with the exception of **2c**, while for the symmetrical alkynes **2a** and **2b**, the difference in this bond length is less than 0.03 Å. The effect of asymmetry in the alkyne is also apparent in **2g$_3$**.

Conclusions

The cluster [Cp*IrRu$_3$(μ-H)$_2$(CO)$_{10}$] reacts with alkynes under thermal activation to yield butterfly clusters of the general formulae [Cp*IrRu$_3$(CO)$_9$(RCCR′)], but with substantial cluster fragmentation. The reactions did not proceed under photochemical or chemical activation with TMNO (trimethylamine *N*-oxide). However, the thermal activation also led to cluster fragmentation to [Cp*Ir(CO)$_2$] and alkyne substituted triruthenium clusters such as **4** and **5**, or the iridium-diruthenium clusters **3**. The yields of these decomposition products can be quite high; over 50% in the case of the combined yields of **3a** and **4a**, and accounted for the observed low yields of the clusters **2**.

The binding of the alkyne also appears to be highly stereoselective, with a general preference towards the stereoisomer in which the alkyne is aligned parallel to an Ru–Ir hinge, and with the bulkier substituent oriented away from the Cp*Ir moiety in the case of unsymmetrical alkynes. A notable exception is observed in the case of phenylacetylene, for which all three possible isomers are observed to be in equilibrium, with the isomer in which the alkyne is aligned parallel to an Ru–Ru hinge being the thermodynamically most stable.

Our results thus represent a map of the possibility of stereoselective binding of alkynes in such heteronuclear clusters. The high stereoselectivity exhibited in some cases suggests that such clusters may be useful in the stereocontrol of reactions with alkynes, and our future work will be directed towards that.

Table 2. Common atomic numbering scheme and selected bond lengths [Å] for **2a**–**c**, **2e**, **2f**, **2g$_2$** and **2g$_3$**.

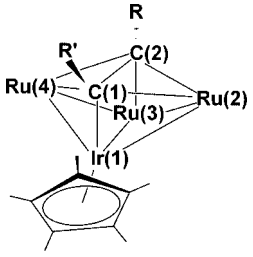

	2a R = R′ = Ph	**2b** R = R′ = Et	**2c** R = *t*Bu R′ = Me	**2e** R = $SiMe_3$ R′ = H	**2f** R = $SiEt_3$ R′ = H	**2g$_2$** R = H R′ = Ph	**2g$_3$**[a] R = Ph R′ = H
Ir(1)–Ru(2)	2.6858(5)	2.6542(3)	2.6699(3)	2.6734(4)	2.6836(8)	2.6545(10)	2.7360(8)
Ir(1)–Ru(3)	2.7997(5)	2.8019(3)	2.8078(3)	2.7964(3)	2.7864(8)	2.7865(11)	2.7890(9)
Ir(1)–Ru(4)	2.6435(5)	2.6594(3)	2.6456(3)	2.6840(4)	2.6845(8)	2.6980(10)	2.7380(10)
Ru(2)–Ru(3)	2.7011(7)	2.6979(4)	2.6903(4)	2.7054(4)	2.7033(10)	2.7266(14)	2.7136(7)
Ru(3)–Ru(4)	2.7075(7)	2.6921(4)	2.6947(4)	2.7132(5)	2.6987(11)	2.7071(13)	2.7571(9)
Ir(1)–C(1)	2.059(6)	2.057(3)	2.053(3)	2.023(4)	2.026(9)	2.047(11)	2.163(10)
Ru(2)–C(1)	2.258(6)	2.270(3)	2.246(3)	2.202(4)	2.197(9)	2.236(11)	2.147(10)
Ru(4)–C(1)	2.261(6)	2.242(3)	2.286(3)	2.186(4)	2.203(9)	2.240(11)	2.237(10)
Ru(2)–C(2)	2.230(5)	2.260(3)	2.312(3)	2.241(4)	2.257(9)	2.220(12)	2.103(8)
Ru(4)–C(2)	2.265(6)	2.254(3)	2.296(3)	2.259(4)	2.255(9)	2.214(11)	2.203(9)
Ru(3)–C(2)	2.170(6)	2.184(3)	2.224(3)	2.178(4)	2.203(9)	2.139(12)	2.148(9)
C(1)–C(2)	1.470(8)	1.458(5)	1.457(5)	1.454(5)	1.444(2)	1.477(16)	1.477(13)

[a] For **2g$_3$**, interchange Ir(1) with Ru(2).

Experimental Section

All reactions were carried out using standard Schlenk techniques under nitrogen. Solvents used in reactions were of AR grade, and were dried, distilled and kept under argon in flasks fitted with Teflon valves prior to use. The products were generally separated by thin-layer chromatography (TLC), using plates coated with silica gel 60 F254 of 0.25 mm or 0.5 mm thickness and extracted with hexane or dichloromethane. Infrared spectra were recorded as hexane solutions unless otherwise stated with a Bio-Rad FTS 165 FTIR spectrometer at a resolution of 1 cm^{-1} using a solution cell with NaCl windows of path length 0.1 mm. NMR spectra were acquired with a Bruker ACF 300 MHz as $CDCl_3$ solutions unless otherwise stated. Chemical shifts reported are referenced to residual protons of the solvent. Mass spectra were collected using the Fast Atom Bombardment (FAB) technique and were carried out with a Finnigan MAT95XL-T mass spectrometer normally with 3-nitrobenzyl alcohol matrix at the National University of Singapore mass spectrometry laboratory. Microanalyses were carried out by the microanalytical laboratory at the National University of Singapore. GC analyses were carried out with an Agilent GC-MS consisting of a GC 6890 MS 5973 equipped with an HP-1 column (300 mm × 0.25 mm × 0.25 μm). In photochemical reactions, UV irradiation was performed with a Hanovia 450 W UV lamp (λ_{max} = 254 nm). The cluster **1** was prepared according to published procedures.[24]

Reaction of 1 with Alkynes: In a typical reaction, cluster **1** (10.0 mg, 10.0 μmol), PhCCPh (2.5 mg, 10 μmol) and hexane (20 mL) were placed in a Carius tube fitted with a teflon valve, and the solution degassed by three freeze-pump-thaw cycles. The reaction was then heated in an oil-bath at 90 °C for 6 h. After removal of the solvent and volatiles under reduced pressure, the residue was redissolved in a minimum volume of dichloromethane and chromatographed on silica-gel TLC plates with 100% hexane as eluent. The analytical and spectroscopic data for the products are given in Table 3. Diffraction quality crystals were grown from hexane by slow cooling.

Thermolysis of 2a and 2b: Cluster **2a** (6.7 mg, 6.0 μmol) and hexane (20 mL) were placed in a Carius tube fitted with a Teflon valve, and the reaction mixture degassed by three freeze-pump-thaw cycles. The mixture was then heated at 90 °C for 7 h. Chromatographic separation of the mixture on silica-gel TLC plates using hexane as eluent afforded three bands. These were, in order of elution, unreacted **2a** (2.0 mg, 30%), **3a** (2.5 mg, 40%), and **1** (0.5 mg, 8%), identified by their IR spectra.

Heating **2b** (8.4 mg, 8.0 μmol) under the same conditions followed by a similar work-up afforded **2b** (3.3 mg, 40%), **3b** (2.4 mg, 35%), and **1** (0.6 mg, 7%).

Photolysis of 2a and 2b: A hexane solution of **2a** (6 mg, 6.0 μmol) was photolysed in a quartz Carius tube under UV light for 7 h. Chromatographic separation of the mixture on silica-gel TLC

Table 3. Spectroscopic and analytical data for the reaction products.

	IR, $\nu_{(CO)}$ [cm^{-1}]	^{1}H NMR, δ [ppm]	Elemental analysis calculated (found)	MS, M^+ found (calculated)
2a	2067 m, 2046 vs, 2023 s, 1994 s, 1973 m	7.13–6.85 (m, 10 H, Ph), 2.07 (s, 15 H, Cp*)	C 37.32 (37.59), H 2.36 (2.04)	1060.8 (1060.9)
2b	2062 m, 2038 vs, 2018 s, 1988 s, 1971 m	(C_6D_6) 2.85 (q, $^3J_{HH}$ = 7.4 Hz, 2 H, $CH_3CH_2CCCH_2CH_3$), 2.61 (q, $^3J_{HH}$ = 7.4 Hz, 2 H, $CH_3CH_2CCCH_2CH_3$), 1.76 (s, 15 H, Cp*), 1.21 (t, $^3J_{HH}$ = 7.4 Hz, 3 H, $CH_3CH_2CCCH_2CH_3$), 0.97 (t, $^3J_{HH}$ = 7.4 Hz, 3 H, $CH_3CH_2CCCH_2CH_3$)	C 31.09 (31.25), H 2.59 (2.51)	964.8 (964.9)
2c	2060 m, 2037 vs, 2027 (sh), 2015 s, 1986 s, 1968 m	2.73 (s, 3 H, CH_3), 2.08 (s, 15 H, Cp*), 1.45 (s, 9 H, *t*Bu)	C 31.87(32.33), H 2.69 (1.98)	980.9 (978.9)
2e	2064 m, 2041 vs, 2016 s, 1991 s, 1973 m	10.53 (s, 1 H, ≡CH), 2.07 (s, 15 H, Cp*), 0.25 (s, 9 H, $SiMe_3$)	C 29.36 (29.54), H 2.55 (2.44)	979.5 (980.9)
2f	2062 m, 2039 vs, 2015 s, 1989 s, 1972 m	(C_6D_6) 10.51 (s, 1 H, ≡CH), 1.72 (s, 15 H, Cp*), 1.09 (q, 6 H, CH_2), 0.92 (t, 9 H, CH_3)	C 32.18 (31.70), H 3.05 (3.16)	1023.6 (1023.0)
2g$_1$	2070 m, 2048 vs, 2024 vs, 1996 s, 1960 w	(C_6D_6) 10.58 (s, 1 H, ≡CH), 7.00–7.77 (m, 5 H, Ph), 1.82 (s, 15 H, Cp*)	low yield	987.7920 (987.7945)
2g$_2$	2069 vs, 2048 vs, 2036 s, 2024 s, 2016 m, 1995 s	(C_6D_6) 11.37 (s, 1 H, ≡CH), 7.00–7.77 (m, 5 H, Ph), 1.87 (s, 15 H, Cp*)	low yield	987.7908 (987.7945)
2g$_3$	2071 vs, 2048 vw, 2031 vs, 2019 vs, 2001 m, 1991 m, 1981 w, 1973 mw, 1960 m, 1950 w	(C_6D_6) 9.44 (s, 1 H, ≡CH), 7.75–6.60 (m, 5 H, Ph), 1.16 (s, 15 H, Cp*)	C 32.93 (33.04), H 2.15 (2.09)	986.0 (987.8)
3a	2065 s, 2032 vs, 1992 m, 1963 m, 1846 br.	7.12–6.88 (m, 10 H, Ph), 1.87 (s, 15 H, Cp*)	C 41.19 (40.71), H 2.79 (2.71)	905.8 (903.9)
3b	2060 s, 2027 vs, 1989 vs, 1962 m, 1834 br.	(C_6D_6) 2.65 (dq, $^3J_{HaHc}$ = $^3J_{HbHc}$ = 7.4 Hz, 2 H, $CH_{3c}CH_aH_bCCCH_{a'}H_{b'}CH_{3c'}$), 2.47 (dq, $CH_{3c}CH_aH_bCCCH_{a'}H_{b'}CH_{3c'}$, $^3J_{Ha'Hc'}$ = 7.4 Hz, 1 H), 2.27 (dq, $^3J_{Hb'Hc'}$ = 7.4 Hz, 1 H, $CH_{3c}CH_aH_bCCCH_{a'}H_{b'}CH_{3c'}$), 1.67 (s, 15 H, Cp*), 1.24 (t, $^3J_{HH}$ = 7.4 Hz, 3 H, $CH_{3c}CH_aH_bCCCH_{a'}H_{b'}CH_{3c'}$), 1.15 (t, $^3J_{HH}$ = 7.4 Hz, 3 H, $CH_{3c}CH_aH_bCCCH_{a'}H_{b'}CH_{3c'}$)	C 34.20 (34.45), H 3.12 (2.99)	807.9 (807.8)

Table 4. Crystal and refinement data for **2a**–**c**, **2e** and **2f**.

Compound	**2a**	**2b**	**2c**	**2e**	**2f**
Empirical formula	$C_{33}H_{25}IrO_9Ru_3$	$C_{25}H_{25}IrO_9Ru_3$	$C_{26}H_{27}IrO_9Ru_3$	$C_{24}H_{25}IrO_9Ru_3Si$	$C_{27}H_{31}IrO_9Ru_3Si$
Formula mass	1060.94	964.86	978.89	980.94	1023.02
Crystal system	monoclinic	monoclinic	monoclinic	monoclinic	orthorhombic
Space group	$P2_1/c$	$P2_1/n$	$P2_1/n$	$P2_1/c$	$Pbca$
Unit cell dimensions [Å, °]	a = 14.0776(5)	a = 9.6671(4)	a = 10.7358(3)	a = 9.3772(4)	a = 16.5440(7)
	b = 9.6907(3)	b = 15.1800(7)	b = 14.8779(4)	b = 15.5636(7)	b = 17.7258(8)
	c = 23.9906(9)	c = 19.4979(9)	c = 18.1779(5)	c = 20.0285(9)	c = 21.6281(9)
	α = 90	α = 90	α = 90	α = 90	α = 90
	β = 92.603(2)	β = 99.6300(10)	β = 92.2750(10)	β = 93.4090(10)	β = 90
	γ = 90	γ = 90	γ = 90	γ = 90	γ = 90
Volume [Å^3]	3269.5(2)	2820.9(2)	2901.20(14)	2917.8(2)	6342.6(5)
Z	4	4	4	4	8
$\rho_{calcd.}$ [Mg/m^3]	2.155	2.272	2.241	2.233	2.143
Absorption coefficient [mm^{-1}]	5.470	6.326	6.153	6.157	5.670
F(000)	2016	1824	1856	1856	3904
Crystal size [mm]	0.22 × 0.16 × 0.10	0.32 × 0.24 × 0.20	0.34 × 0.26 × 0.14	0.30 × 0.22 × 0.08	0.12 × 0.04 × 0.01
θ range for data collection [°]	2.18–26.37	2.12–26.37	2.17–30.01	2.04–29.55	2.25–26.37
Reflections collected	25711	41944	24638	22671	49894
Independent reflections	6683 [R(int) = 0.0444]	5761 [R(int) = 0.0303]	8188 [R(int) = 0.0277]	7440 [R(int) = 0.0326]	6478 [R(int) = 0.1287]
Data/restraints/parameters	6683/0/420	5761/0/350	8188/0/361	7440/0/355	6478/0/381
Goodness-of-fit on F_2	1.107	1.090	1.050	1.036	1.034
Final R indices [$I > 2\sigma(I)$]	R_1 = 0.0399,	R_1 = 0.0213,	R_1 = 0.0277,	R_1 = 0.0307,	R_1 = 0.0504,
	wR_2 = 0.0842	wR_2 = 0.0520	wR_2 = 0.0621	wR_2 = 0.0645	wR_2 = 0.0870
R indices (all data)	R_1 = 0.0460,	R_1 = 0.0231,	R_1 = 0.0318,	R_1 = 0.0363,	R_1 = 0.0898,
	wR_2 = 0.0867	wR_2 = 0.0528	wR_2 = 0.0637	wR_2 = 0.0666	wR_2 = 0.0996
Largest diff. peak/hole [e·Å^{-3}]	1.836/–0.755	1.141/–0.575	1.570/–0.847	1.127/–0.796	1.276/–0.871

Table 5. Crystal and refinement data for **2g$_2$**, **2g$_3$**, **3a**, **3b** and **4b**.

Compound	**2g$_2$**	**2g$_3$**	**3a**	**3b**	**4b**
Empirical formula	$C_{27}H_{21}IrO_9Ru_3$	$C_{27}H_{21}IrO_9Ru_3$	$C_{31}H_{25}IrO_7Ru_2$	$C_{23}H_{25}IrO_7Ru_2$	$C_{20}H_{20}O_8Ru_3$
Formula mass	984.85	984.85	903.85	807.77	691.57
Crystal system	monoclinic	monoclinic	monoclinic	orthorhombic	monoclinic
Space group	$P2_1/c$	Cc	$P2_1/n$	$Pbca$	$P2_1/n$
Unit cell dimensions [Å, °]	a = 16.2320(8)	a = 19.9566(11)	a = 10.0663(3)	a = 9.9869(3)	a = 9.7768(5)
	b = 13.0498(7)	b = 9.9529(4)	b = 19.1058(6)	b = 16.0665(4)	b = 18.1206(9)
	c = 13.5375(7)	c = 16.6241(7)	c = 15.2570(6)	c = 30.8922(8)	c = 12.9616(6)
	α = 90	α = 90	α = 90	α = 90	α = 90
	β = 90.843(2)	β = 119.6740(10)	β = 97.0130(10)	β = 90	β = 93.1270(10)
	γ = 90	γ = 90	γ = 90	γ = 90	γ = 90
Volume [Å^3]	2867.3(3)	2868.9(2)	2912.34(17)	4956.8(2)	2292.88(19)
Z	4	4	4	8	4
$\rho_{calcd.}$ [Mg/m^3]	2.281	2.280	2.061	2.165	2.003
Absorption coefficient [mm^{-1}]	6.227	6.223	5.628	6.599	1.993
F(000)	1856	1856	1728	3072	1344
Crystal size [mm]	0.13 × 0.12 × 0.02	0.20 × 0.08 × 0.06	0.22 × 0.10 × 0.08	0.18 × 0.16 × 0.02	0.34 × 0.24 × 0.04
θ range for data collection [°]	2.00–26.37	2.35–28.28	2.13–24.71	2.49–26.37	2.25–26.37
Reflections collected	36509	42704	23408	40378	31805
Independent reflections	5864 [R(int) = 0.0848]	3553 [R(int) = 0.0777]	4960 [R(int) = 0.0449]	5060 [R(int) = 0.0593]	4682 [R(int) = 0.0335]
Data/restraints/parameters	5864/1/370	3553/8/369	4960/0/375	5060/0/305	4682/0/284
Goodness-of-fit on F_2	1.386	0.929	1.064	1.195	1.128
Final R indices [$I > 2\sigma(I)$]	R_1 = 0.0733,	R_1 = 0.0297,	R_1 = 0.0333,	R_1 = 0.0405,	R_1 = 0.0298,
	wR_2 = 0.1350	wR_2 = 0.0810	wR_2 = 0.0746	wR_2 = 0.0776	wR_2 = 0.0722
R indices (all data)	R_1 = 0.0826,	R_1 = 0.0302,	R_1 = 0.0374,	R_1 = 0.0487,	R_1 = 0.0330,
	wR_2 = 0.1383	wR_2 = 0.0817	wR_2 = 0.0765	wR_2 = 0.0803	wR_2 = 0.0739
Largest diff. peak/hole [e·Å^{-3}]	2.152/ –2.267	1.623/–1.490	2.138/–0.488	1.214/–1.151	1.041/–0.341

plates using hexane as eluent afforded **2a** (2.3 mg, 40%), **3a** (2 mg, 30%), and **1** (0.4 mg, 6%).

Irradiation of **2b** (8.5 mg, 9.0 μmol) under the same conditions, followed by a similar work-up, afforded **2b** (3.4 mg, 40%), **3b** (2.5 mg, 38%), and **1** (0.5 mg, 6%).

Reaction of 1 with 1-Hexene: Cluster **1**, (5 mg, 5.0 μmol) and 1-hexene (10 μL, 80 μmol) in deuterated toluene (0.5 mL) were stirred in an NMR tube and the reaction monitored by ^{1}H NMR over a period of 7 h. Signals due to a mixture of 2- and 3-hexene were observed in the ^{1}H NMR spectrum, suggesting isomerisation of the

alkene. The infrared spectrum of the reaction mixture showed that cluster **1** remained mainly unchanged.

X-Ray Crystal Structure Determinations: Crystals were mounted on quartz fibres. X-ray data were collected with a Bruker AXS APEX system, using Mo-K_α radiation, at 223 K with the SMART suite of programs.[25] Data were processed and corrected for Lorentz and polarisation effects with SAINT,[26] and for absorption effects with SADABS.[27] Structural solution and refinement were carried out with the SHELXTL suite of programs.[28] Crystal and refinement data are summarised in Table 4 and Table 5.

The structures were solved by direct methods to locate the heavy atoms, followed by difference maps for the light, non-hydrogen atoms. All non-hydrogen atoms were generally given anisotropic displacement parameters in the final model. Organic hydrogen atoms were placed in calculated positions and refined with a riding model. Compound $\mathbf{2g_3}$ was refined as a racemic twin.

CCDC-283339 to -283350 contain the supplementary crystallographic data for this paper. These data can be obtained free of charge from The Cambridge Crystallographic Data Centre via www.ccdc.cam.ac.uk/data_request/cif.

Acknowledgments

This work was supported by the National University of Singapore (Research Grant No. R143-000-190-112) and one of us (P. S.) thanks the University for a Research Scholarship.

[1] R. D. Adams, F. A. Cotton, *Catalysis by Di- and Polynuclear Metal Cluster Complexes*, Wiley: New York, **1998**.
[2] a) E. Sappa, A. Tiripicchio, P. Braunstein, *Chem. Rev.* **1983**, *83*, 203; b) N. T. Allison, J. R. Fritch, K. P. C. Vollhardt, E. C. Walborsky, *J. Am. Chem. Soc.* **1983**, *105*, 1384; c) A. D. Clauss, J. R. Shapley, C. N. Wilker, R. Hoffmann, *Organometallics* **1984**, *3*, 619; d) E. Roland, H. Vahrenkamp, *Organometallics* **1983**, *2*, 183; e) E. L. Muetterties, *Angew. Chem. Int. Ed. Engl.* **1978**, *90*, 577; f) E. L. Muetterties, T. N. Rhodin, E. Band, C. F. Bruker, W. R. Pretzer, *Chem. Rev.* **1979**, *79*, 91.
[3] A. Choualeb, P. Braunstein, J. Rose, R. Welter, *Inorg. Chem.* **2004**, *43*, 57.
[4] E. Sappa, A. Tiripicchio, A. J. Carty, G. E. Toogood, *Prog. Inorg. Chem.* **1987**, *35*, 437.
[5] a) E. W. Abel, F. G. A. Stone, G. Wilkinson, *Comprehensive Organometallic Chemistry II*, 1st ed., Pergamon: Oxford, New York, **1995**; b) L. F. Dahl, D. L. Smith, *J. Am. Chem. Soc.* **1962**, *84*, 2450; c) R. J. Haines, N. D. C. T. Steen, M. Laing, P. Sommerville, *J. Organomet. Chem.* **1980**, *198*, C72.
[6] K. Wade, *Adv. Inorg. Chem. Radiochem.* **1976**, *18*, 1.
[7] J. A. Cabeza, P. García-Alvarez, E. Pérez-Carreño, *Organometallics* **2005**, *24*, 2000.
[8] a) M. Cazanoue, N. Lugan, J. J. Bonnet, R. Mathieu, *Organometallics* **1988**, *7*, 2480; b) V. Ferrand, G. Süss-Fink, A. Neels, H. Stoeckli-Evans, *J. Chem. Soc., Dalton Trans.* **1998**, 3825; c) V. Ferrand, G. Süss-Fink, A. Neels, H. Stoeckli-Evans, *Eur. J. Inorg. Chem.* **1999**, 853.
[9] J. R. Fox, W. L. Gladfelter, G. L. Geoffroy, I. Tavanaiepour, S. Abdel-Mequid, V. W. Day, *Inorg. Chem.* **1981**, *20*, 3230.
[10] J. L. Le Grand, W. E. Lindsell, K. J. McCullough, C. H. McIntosh, A. G. Meiklejohn, *J. Chem. Soc., Dalton Trans.* **1992**, 1089.
[11] a) M. V. Capparelli, Y. De Sanctis, A. J. Arce, *Acta Crystallogr. Sect. C: Cryst. Struct. Commun.* **1995**, *51*, 1819; b) S. Aime, L. Milone, D. Osella, M. Valle, *J. Chem. Res. Synop.* **1978**, 77.
[12] Crystal data for **5a**: $P2_1/c$, a = 9.5075(4) Å; b = 18.5955(9) Å; c = 18.3912(8) Å; β = 95.457(2)°. Ref.[11a] $P2_1/c$, a = 9.556(3) Å, b = 18.694(4) Å, c = 18.465(2) Å, β = 95.77(1)°.
[13] For examples see: a) P. Braunstein, J. Rose, O. Bars, *J. Organomet. Chem.* **1983**, *252*, C101; b) E. Roland, H. Vahrenkamp, *Organometallics* **1983**, *2*, 1048; c) E. Sappa, A. Tiripicchio, M. T. Camellini, *J. Organomet. Chem.* **1981**, *213*, 175; d) L. Busetto, M. Green, J. A. K. Howard, B. Hessner, J. C. Jeffery, R. M. Mills, F. G. A. Stone, P. Woodward, *J. Chem. Soc., Dalton Trans.* **1981**, 1101.
[14] M. Smith, J. March, *March's Advanced Organic Chemistry: Reactions, Mechanisms and Structure*, 5th ed., John Wiley & Sons: New York, Singapore, **2001**.
[15] ν_{CO} (hex): 2064 m, 2042 vs, 2028 (sh), 2019 s, 1991 s, 1974 m cm^{-1}.
[16] A. J. Edwards, N. E. Leadbeater, J. Lewis, P. R. Raithby, *J. Chem. Soc., Dalton Trans.* **1995**, 3785.
[17] Crystal data: space group $P\bar{1}$; a = 9.0738(7) Å; b = 9.1688(7) Å; c = 13.0136(9) Å; α = 93.546(1)°; β = 107.152(1)°; γ = 97.881(1)°. Lit. values: $P\bar{1}$, a = 9.1554(10) Å; b = 9.2373(10) Å; c = 13.1229(10) Å; α = 92.135(10)°; β = 106.738(10)°; γ = 98.483(10)°.
[18] F. J. Zuno-Cruz, A. L. Carrasco, M. J. Rosales-Hoz, *Polyhedron* **2002**, *21*, 1105.
[19] J. J. Schneider, M. Nolte, C. Krueger, *J. Organomet. Chem.* **1991**, *403*, C4.
[20] H. Bantel, A. K. Powell, H. Vahrenkamp, *Chem. Ber.* **1990**, *123*, 661.
[21] a) S. Haak, G. Süss-Fink, A. Neels, H. Stoeckli-Evans, *Polyhedron* **1999**, *18*, 1675; b) G. Süss-Fink, S. Haak, V. Ferrand, H. Stoeckli-Evans, *J. Chem. Soc., Dalton Trans.* **1997**, 3861.
[22] a) A. Fumagalli, M. C. Malatesta, M. Vallario, G. Ciani, M. Moret, A. Sironi, *J. Cluster Sci.* **2001**, *12*, 187; b) H. C. Bottcher, M. Graf, K. Merzweiler, C. Wagner, *Polyhedron* **2000**, *19*, 2593; c) G. Süss-Fink, S. Haak, V. Ferrand, H. Stoeckli-Evans, *J. Mol. Catal. A* **1999**, *143*, 163; d) J. R. Galsworthy, C. E. Housecroft, D. M. Matthews, R. Ostrander, A. L. Rheingold, *J. Chem. Soc., Dalton Trans.* **1994**, 69; e) L. Y. Hsu, W. L. Hsu, D. A. McCarthy, J. A. Krause, J. H. Chung, S. G. Shore, *J. Organomet. Chem.* **1992**, *426*, 121.
[23] a) M. R. Churchill, J. P. Hutchinson, *Inorg. Chem.* **1978**, *17*, 3528; b) V. J. Johnston, F. W. B. Einstein, R. K. Pomeroy, *Organometallics* **1988**, *7*, 1867; c) M. R. Churchill, F. J. Hollander, J. P. Hutchinson, *Inorg. Chem.* **1977**, *16*, 2655.
[24] P. Srinivasan, W. K. Leong, *J. Organomet. Chem.*, manuscript accepted.
[25] SMART version 5.628, Bruker AXS Inc., Madison, Wisconsin, USA, **2001**.
[26] SAINT+ version 6.22a, Bruker AXS Inc., Madison, Wisconsin, USA, **2001**.
[27] G. M. Sheldrick, SADABS, **1996**.
[28] SHELXTL version 5.1, Bruker AXS Inc., Madison, Wisconsin, USA, **1997**.

Received: September 16, 2005
Published Online: November 15, 2005

